

Mitochondria poised at a fission-fusion balance?: A quantitative assessment of mitochondrial network complexity

Nahuel Zamponi^{1,+,*}, Emiliano Zamponi^{1,+}, Sergio A. Cannas^{2,4}, Orlando V. Billoni^{2,4}, Pablo R. Helguera^{1,4*}, and Dante R. Chialvo^{3,4}

¹Mitochondrial Research Group, Instituto de Investigaciones Médicas Mercedes y Martín Ferreyra y Universidad Nacional de Córdoba (INIMEC-CONICET-UNC), Friuli 2434, (5016) Córdoba, Argentina.

²Facultad de Matemática Astronomía Física y Computación, Universidad Nacional de Córdoba, Instituto de Física Enrique Gaviola (IFEG-CONICET), Ciudad Universitaria. (5000) Córdoba, Argentina.

³Center for Complex Systems and Brain Sciences (CEMSC³), Universidad Nacional de San Martín, Campus Miguelete, 25 de Mayo y Francia (1650), San Martín, Buenos Aires, Argentina.

⁴Consejo Nacional de Investigaciones Científicas y Tecnológicas (CONICET), Godoy Cruz 2290, (1425) Buenos Aires, Argentina.

⁺these authors contributed equally to this work

^{*}nzamponi@immf.uncor.edu, phelguera@immf.uncor.edu

ABSTRACT

Mitochondrial networks have been shown to exhibit a variety of complex behaviors, including cell-wide oscillations of mitochondrial energy states, as well as a phase transition in response to oxidative stress. Since functional status and structural properties are often intertwined, in this work we look at the structural properties of the organelle in normal mouse embryonic fibroblasts, describing its most relevant features. Subsequently we manipulated mitochondrial morphology using two interventions with opposite effects: over-expression of mitofusin 1, a protein that promotes mitochondria fusion, and paraquat treatment, a compound that induces mitochondrial fragmentation due to oxidative stress. Quantitative analysis of the organelle's structural clusters revealed that healthy mitochondrial networks were in a status intermediate between the extremes of highly fragmented and completely fused networks. This was confirmed by a comparison of our empirical findings with those of a recently described computational model of network growth based on fusion-fission balance. These results, offer an objective methodology to parametrize the mitochondrial status under a variety of both physiological and pathological cellular conditions, and overall add weight to the fission-fusion model for the mitochondrial reticulum dynamics.

Mitochondrial networks have been shown to exhibit a variety of complex behaviors, including cell-wide oscillations of mitochondrial energy states, as well as a phase transition in response to oxidative stress. Since functional status and structural properties are often intertwined, in this work we look at the structural properties of the organelle in normal mouse embryonic fibroblasts, describing its most relevant features. Subsequently we manipulated mitochondrial morphology using two interventions with opposite effects: over-expression of mitofusin 1, a protein that promotes mitochondria fusion, and paraquat treatment, a compound that induces mitochondrial fragmentation due to oxidative stress. Quantitative analysis of the organelle's structural clusters revealed that healthy mitochondrial networks were in a status intermediate between the extremes of highly fragmented and completely fused networks. This was confirmed by a comparison of our empirical findings with those of a recently described computational model of network growth based on fusion-fission balance. These results, offer an objective methodology to parametrize the mitochondrial status under a variety of both physiological and pathological cellular conditions, and overall add weight to the fission-fusion model for the mitochondrial reticulum dynamics.

Mitochondria arose around two billion years ago from the engulfment of an α -proteobacterium by a precursor of the modern eukaryotic cell.¹ Subsequent evolution shaped the relation between mitochondria and its host cell, leading to a highly specialization of both morphology and function of this organelle. Long known for its role in ATP production, mitochondria also participates in a myriad of processes such as apoptosis, calcium buffering and phospholipid synthesis, among others.² In addition, complex dynamic patterns occur in mitochondria, including oscillations and phase transitions.^{3,4} Thus, it is not surprising that a variety of functional alterations impact on mitochondrial morphology and viceversa. Although it is accepted that the structural status of the network is a predictor of the functional state of the organelle, only recently detailed quantitative studies of this relation are appearing, mostly due to the inherent difficulty in estimating changes in its complex structure.

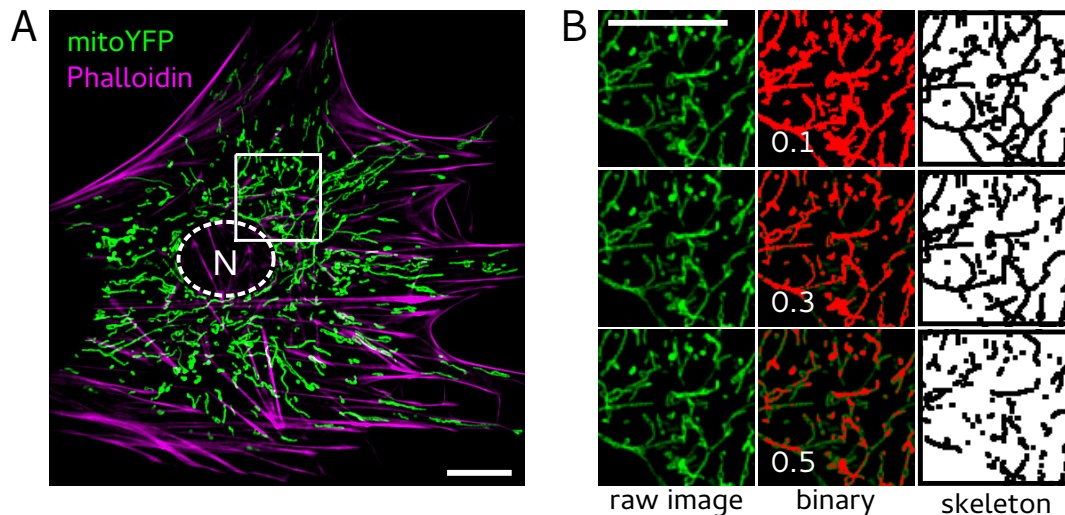


Figure 1. Mitochondrial networks are extracted from confocal microscopy images as the example in Panel A corresponding to a mouse embryonic fibroblast. The mitochondrial network is shown in green and the actin cytoskeleton in magenta. Panel B: Example of the image processing steps used to extract the network from the raw image (left column). First, the images are binarized at increasing threshold values (as the examples for 0.1, 0.3 and 0.5 in the middle column, where red corresponds to pixels above the threshold) and subsequently converted to skeletons of uniform thickness (right column). Scale bars in both panels represent $10\mu\text{m}$.

A typical mitochondria comprises a complex network of tubule-like structures, with fragments of all sizes (ranging from less than $1\mu\text{m}$ to $15\mu\text{m}$ or more).⁵ The current theoretical understanding propose that the network spatial organization is maintained by two opposing processes, fusion and fission, which depending on their relative predominance determine the overall network shape and morphological properties.⁶

The aim of this work is to characterize the structural and topological properties of the mitochondrial network and its modification by two perturbations that target opposing processes, namely extensive fusion or fission. We found that mitochondrial morphology in control cells exhibited distinctive scale-free features, which were disrupted by both experimental manipulations. These observations were consistent with predictions of the Sukhorukov *et al.* model⁷ of network growth where healthy mitochondrial networks are in a critical regime intermediate between the fragmented and fused networks, depending on the predominance of either fusion or fission events.

Results

Determination of the mitochondrial network structure

The complex mitochondrial structure from a mouse embryonic fibroblast (MEF) can be appreciated in the example presented in Figure 1. Panel A shows a typical image obtained from confocal microscopy in which mitochondria is shown in green by expressing mitochondrial targeted yellow fluorescent protein (mYFP) and the actin cytoskeleton is shown in magenta by labelling with a fluorescent conjugate of phalloidin (see Methods). In order to study the rich structure exhibited by the mitochondrial network, the images need to be processed to extract the bare skeleton of the entire mitochondrial network. To that matter, routines from Matlab (Natick, Massachusetts: The MathWorks Inc.) were used in three steps: the first was a thresholding operation over the fluorescence intensity, which accounted for the fact that different cells may produce images of different contrast. The second step produced, for each cell, a binarized image (using *im2bw*) at increasing threshold values. In the third and final step, the binarized image was converted to an skeleton of uniform (one pixel) thickness, (using *bwmorph*) which constituted the data used for further analysis.

Experimental manipulations robustly alter mitochondrial network structure

The status of the mitochondrial network was investigated under control conditions as well as after two experimental manipulations. Mitochondrial network data was obtained from MEFs under normal conditions (control), as well as under mitofusin 1 over-expression (MFN) and paraquat treatment (PRQ). Typical examples of three networks are presented in Figure 2. These manipulations are known, by previous work, to either enhance or impair mitochondrial network connectivity, respectively.

A simple qualitative inspection revealed that, compared with control networks, MFN networks appeared as elongated

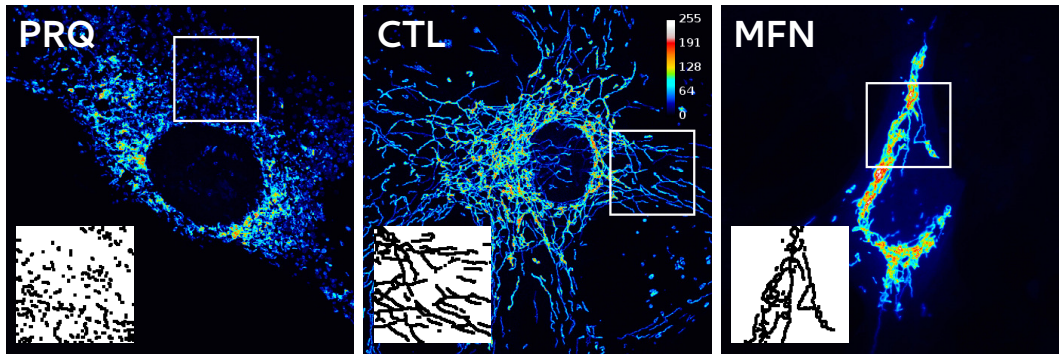


Figure 2. Typical examples of mitochondrial networks extracted under control (CTL, Cell # CTL03) conditions, as well as with the two manipulations studied here: over-expression of mitofusin 1 (MFN, Cell # MFN01) and treatment with paraquat (PRQ, Cell # PRQ05). The insets correspond to the skeletons extracted from the boxed regions (box side = $15\mu\text{m}$). The color scale depicts the fluorescence intensity of mYFP.

strings, while in the case of the PRQ networks the mitochondria seemed fragmented in relatively small patches. In fact, this type of qualitative visual inspection is the approach used routinely to evaluate the status of the mitochondrial networks,^{8–10} counting the relative ratios of cells exhibiting structures different from that of the control cells. It would be desirable to go beyond these qualitative estimations and to develop a quantitative estimation method able to properly track potential changes from normal to abnormal mitochondrial network structure.

Quantification of mitochondrial network structure and topology

The insets in Figure 3 define the network elements measured in each cell, namely the clusters, the number of links (i.e., k , the node degree) and segments; where (following Ref.⁷) 1-1 means a segment that connects two nodes with $k = 1$ and 1-3 refers to those segments connecting a node with $k = 3$ and a node with $k = 1$. The statistics confirmed the impression gotten from the visual inspection of the networks: Figure 3 shows that mitochondrial networks were formed by clusters of all sizes; from the largest ($\sim 10^3\mu\text{m}$) to the smallest one there is a scale free distribution of cluster sizes. As observed in Figure 3 Panel A, the cumulative distribution of cluster sizes of CTL networks laid in between the one of MFN and PRQ networks. This is consistent with the fact that mitofusin 1 over-expression enhances network fusion while the paraquat treatment favors fragmentation. This effect was also apparent when segments statistics were investigated. As indicated by the distributions in panel B the CTL networks exhibited an order of magnitude longer 1-1 segments than the treated networks. The same applies for the 1-3 segments that exhibited again an intermediate behavior compared to treated cells.

To illustrate the typical data obtained on a single cell level, Figure 4 shows the statistics for one cell for each group, as a function of the threshold value used for image binarization. Each of the columns correspond to the results obtained from one cell for each treatment, CTL in the middle, MFN on the right and PRQ on the left. The number of clusters, in all cases, exhibited a non monotonic behavior for increasing thresholds. This is expected, regardless of the nature or origin of the image, anytime a section is made cutting a rough landscape. The position of the curve peak can be useful to make an educated choice of a threshold value which includes the most representative cluster statistics.

The average cluster size $\langle s \rangle$ changed monotonically with the threshold; however, it should be noticed that PRQ values were much smaller than for the other networks. Panels in the middle row show the cumulative distribution of cluster sizes, same statistics seen already in panel A of Figure 3, in this case as a function of a range of threshold values. In search of a well behaved normalizing procedure, we found that the average cluster size $\langle s \rangle$ can be used to normalize the densities, eventually leading to a unique average representative distribution for any threshold value.

Are mitochondrial networks poised at a fission-fusion balance?

The structural and topological changes described in the previous paragraphs were consistent with the molecular mechanisms suggested by the available literature about paraquat^{11,12} and mitofusin 1^{6,13–16} treatments. These ideas propose that a steady state mitochondrial network requires a proper balance of two opposing tendencies, one toward fusing segments and the other to favor fragmentation. Recently, a mathematical model containing explicit variables for these two opposing forces was implemented⁷ (See Methods). In an attempt to further test these interpretations we contrasted some of our experimental results with the predictions of the model. In order to proceed, a bootstrapping approach was required to extract model parameters from the experimental data. First, the order parameter was defined as the ratio of the largest cluster $\langle N_g \rangle$ over the network size N . Then, for a fixed value of c_1 both the order parameter ($\langle N_g \rangle / N$) and the average degree $\langle k \rangle$ as a function of c_2 were numerically

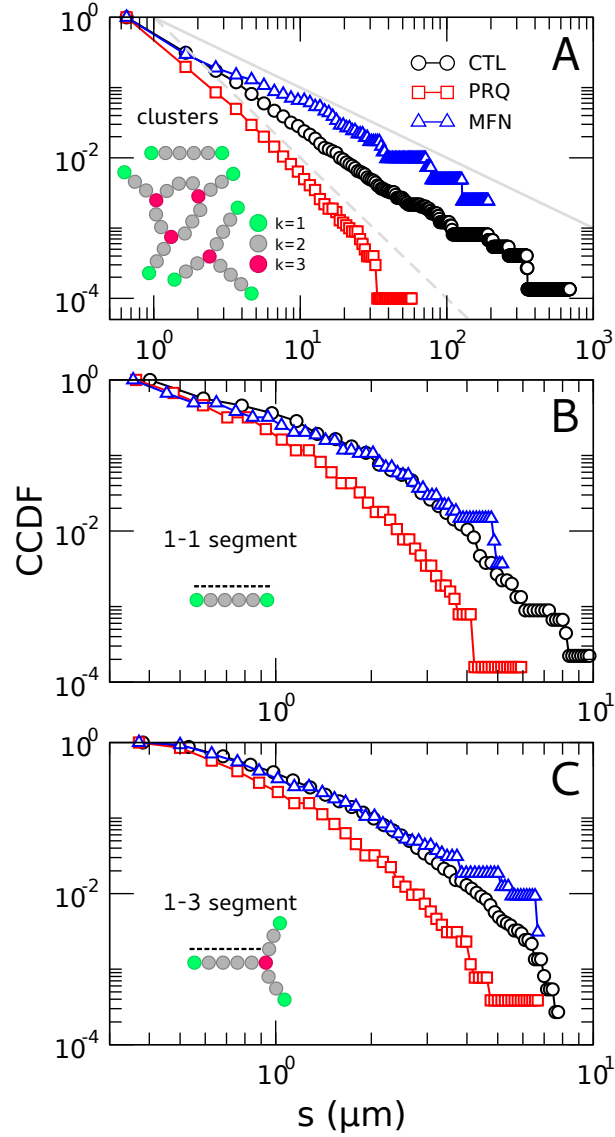


Figure 3. The structural average properties of control mitochondrial networks lie in between those corresponding to excessive fusion or fission. The PRQ treated cells exhibit, on the average, the shortest segments and the smallest clusters while those from the MFN group shows relatively larger clusters and segments. Panel A shows the complementary cumulative distribution functions for clusters sizes; the sizes of open and branched segments are shown in Panels B and C respectively, computed from all data sets in each group ($n=5$, threshold=0.15). While the cluster sizes distribution seems to obey a power law, open and branched segments distributions both show exponential decays. The insets show the definitions for node, degree, clusters and segments.

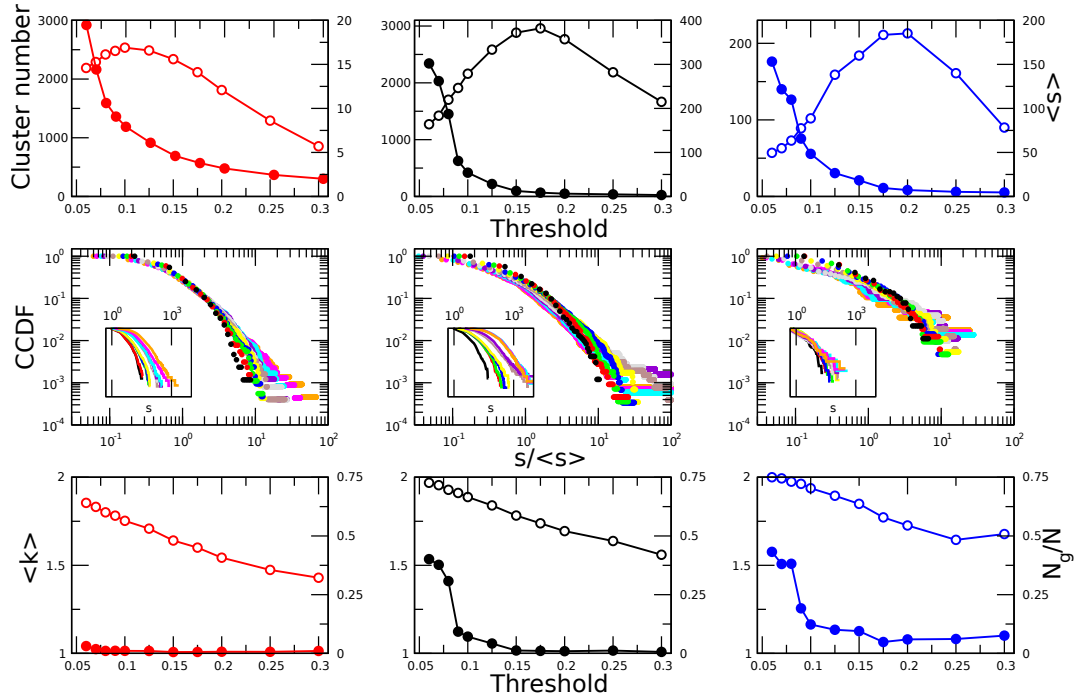


Figure 4. Typical mitochondrial network parameters computed from one cell of each group. Center column corresponds to control cell, left column to PRQ and right column to MFN. The panels in the top row show the number of clusters (empty symbols, left labels) and the mean cluster size (filled symbols, right labels) as a function of the binarization threshold. In the panels of the middle row the cluster cumulative density distributions for each threshold are plotted over-imposed (colors denote the different threshold values). Notice that by normalizing cluster size with its mean value $\langle s \rangle$, distributions computed with different thresholds collapse approx. to the same function. The insets show the unnormalized distributions. The panels in the bottom row depict, as a function of the binarization threshold, the mean degree (empty symbols, left labels) and the size of the largest cluster (filled symbols, right labels) of the network. Data correspond to cell codes PRQ03, CTL03 & MFN03.

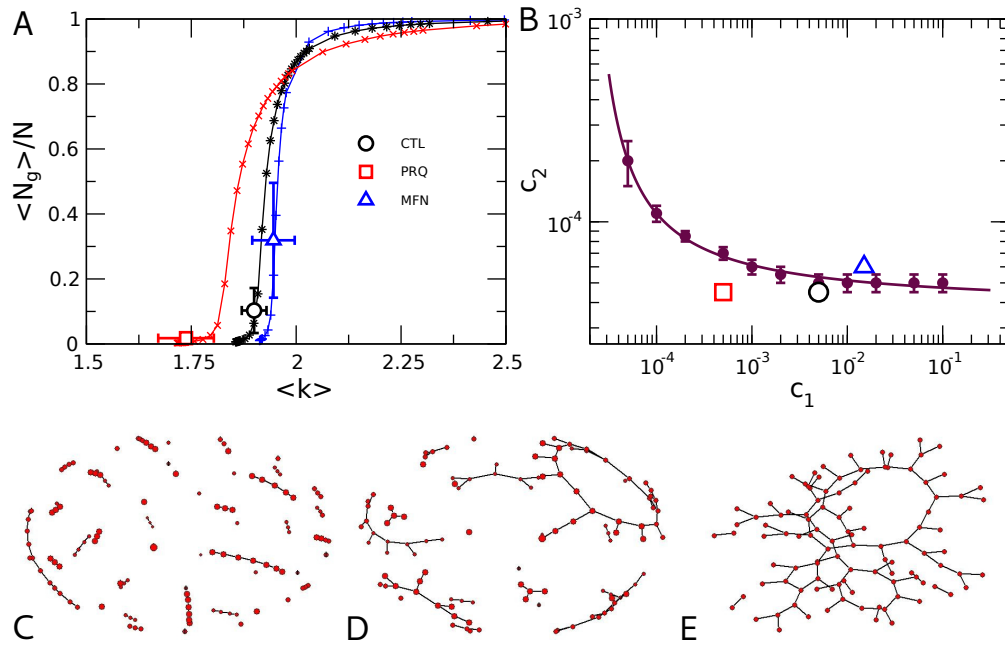


Figure 5. Comparison of the present experimental results with those of Sukhorukov' *et al.* model. (A) Model parameters extracted iteratively from the experimental data. Open symbols and error bars correspond to means and standard deviations of all cells for the CTL, PRQ and MFN groups (for a binarization threshold = 0.15). Each point of the extracted curves corresponds to a unique pair of values (c_1, c_2) . (B) Phase diagram of the model in the (c_1, c_2) space. Filled symbols and the continuous line correspond to the location of the phase transition. The three open symbols (labeled PRQ, CTL, MFN) correspond to the parameter values extracted from the experimental data as shown in (A). Panels C, D and E show a graphical representation of the typical networks simulated using the three derived (c_1, c_2) values.

computed. Next, for every value of c_1 , $\langle N_g \rangle / N$ was plotted parametrically by varying c_2 , as a function of $\langle k \rangle$.

Continuous lines in panel A of Figure 5 are an example of those curves. It could be observed that, at least for the parameters region of interest, each point of the curves corresponded to a unique pair of values (c_1, c_2) (see Supp. Mat.). This allowed us to roughly associate model parameters values to the experimental data. The symbols in the figure correspond to an average of $\langle N_g \rangle / N$ and $\langle k \rangle$ over different cell groups. In panel B the phase diagram in the (c_1, c_2) space is illustrated. The filled symbols (with error bars) correspond to the maxima in the mean cluster size $\langle s \rangle$ (see Supp. Mat.). The continuous line is a non linear fitting to the points and represents a reference to the eye for the location of the phase transition. The three symbols correspond to the parameter values extracted from the experimental data in the three conditions shown in (A). The graphs on panels C, D and E show examples of the typical networks constructed with the model using the three derived empirical values (i.e., the points in Panel B labeled PRQ, CTL, MFN respectively). The results obtained from the numerical exercise with the model strengthened the rationale about the forces supposedly shaping the mitochondrial network, which are consistent with the experimental manipulations used in the present work.

Discussion

The main findings of the present study can be summarized in three aspects. First, regardless of mitochondrial network complexity, the approach described here allows for a straightforward quantitative estimation of the network state. Second, using two experimental manipulations, mitofusin 1 over-expression and treatment with paraquat, we emulated the physical boundaries of the mitochondrial network plasticity, and demonstrated that its transitions can be objectively tracked over the different statistical properties of the network. Finally, when the experimental data is contrasted with the recently published Sukhorukov *et al.* mathematical model, a good agreement is found between the predictions of the model for the mitochondrial network changes. Specifically, the empirical network configurations were founded at parameter regions predicted by the model, adding support for the suggested percolation phase transition in the mitochondrial reticulum.⁷

Despite the encouraging findings, these results should be considered a proof of concept, and caution should be taken regarding sensitive limitations inherent to both type and quality of cells, image processing and the number of cells reported. We have already applied successfully this approach in other cell types, such as human fibroblasts, rat neurons and glial cells, as

well as several immortal cell lines like NIH313, HEK and CHO (to be reported elsewhere). From a methodological point of view, the most important concern with image processing is to minimize the background fluorescence noise, otherwise at very low threshold values numerous very small clusters contaminate the statistic.

We expect that the present approach can be fruitfully used to monitor developmental and pathological changes in mitochondrial networks, as well as a quantitative description of cell recovery from damage. In that sense, research carried in Down Syndrome human cells has shown that the specific structural alterations of mitochondria can be partially reverted by over-expressing mitofusin 1.¹⁷ We believe that quantitative tools such as the one presented here can be helpful in the description of the effects of different treatments on dysfunctional mitochondria. Moreover, the same quantitative analysis could be of value in the description of the participation of the different elements of the cytoskeleton in mitochondrial structure maintenance and dynamics.¹⁰

Methods

Cell culture

Mouse Embryonic Fibroblasts (MEFs) were obtained as described by Xu et al. (2005).¹⁸ Briefly, 13.5 days old mouse embryos were extracted from the mother uterus, rinsed with PBS and placed on a petri dish. The head and red organs were discarded, and the remaining body was again rinsed with PBS and placed on a new petri dish. Using shaving blades, the tissue was chopped into little pieces, until it was able to pipet, and trypsinized 15 sec. at 37 C (PBS 10% Trypsin). Trypsin reaction was quenched with serum-containing media and the whole mixture was centrifuged 5' at 2000 rpm. The supernatant was discarded and the pelleted cells were resuspended in DMEM with 10% SFB, 1% GlutaMax and 1% Non-essential Amino Acids. A volume equivalent to 4 embryos of cell-containing media was seeded on 175 cm² culture bottles and were allowed to grow for 48 h. C57BL6 mice were obtained from the Animal Facility of Instituto de Investigaciones Médicas Mercedes y Martin Ferreyra (INIMEC-CONICET-UNC). All animal procedures were performed in strict accordance with the guidelines of the Institutional Council of Animal Care (CICUAL-INIMEC), and efforts were made to minimize the number of manipulations and animals used.

Mitochondrial network morphology manipulation and cell imaging

The mitochondrial reticulum was visualized by lentiviral infection. Lentiviruses were produced as described by Baloh *et al.*¹⁹ Briefly, human embryonic kidney (HEK) 293T cells were plated onto six-well plates and transfected using Lipofectamine 2000 (Invitrogen) reagent with a polymerase-coding vector (REV), a packaging vector (8.71), an envelope vector (VSVG), and a shuttle vector encoding the mitochondrial-targeted yellow fluorescent protein (mitoYFP). Media was changed once at 12 h and collected at 48 and 72 h, pooled, and applied directly to MEFs cultures. Posterior manipulations of the mitochondrial network morphology were accomplished in two ways: 1) to induce mitochondrial fragmentation, the mitoYFP-expressing MEF cultures were treated with 200 μ M Paraquat (Sigma-Aldrich) for 24 hours, and 2) to induce mitochondrial over-fusion, cultures were transfected (Lipofectamine 2000, Invitrogen) with a plasmid encoding the sequence of the human Mitofusin 1 gene (MFN1, Addgene). Once ready, cells were fixed with 4% PFA in 4% sucrose-containing PBS. F-actin staining was performed on fixed cells using Alexa 546-phalloidin (Molecular Probes), according to the manufacturer's protocol. In all cases, image acquisition was achieved using a Olympus IX81 inverted microscope equipped with a Disk Spinning Unit (DSU), epifluorescence illumination (150 W Xenon Lamp), and a microprocessor. MEFs were imaged using a 60 x oil immersion objective, an ORCA AG (Hamamatsu) CCD camera and OSIS software.

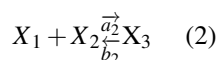
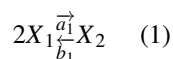
Image analysis

All routines used for the analysis and image processing were written in Matlab (The MathWorks, Natick, MA). As explained above, the mitochondrial network structures were extracted from the micrographs of fluorescence tagged mitochondria. Because of unavoidable difference in images contrast, a normalization procedure need to be use to extract the mitochondrial networks and compare across cells. First, individual 8-bit images were converted to binary (i.e., black & white) for different threshold values of intensity using the Matlab routine *im2bw*. For each threshold value (range 0-1) the skeleton (i.e., the image reduced to a trace of one- pixel thickness) was extracted using the Matlab routine *bmorph*. Subsequently, clusters were extracted using the Matlab routine *bwlabel*. The algorithm define a cluster as those pixels connected with at least one of the eight nearest neighbors. The degree of each node was computed using a numerical routine that inspects each node and counts the number of nearest neighbors.

Sukhorukov *et al.* Model

Numerical simulations were conducted using the model of Sukhorukov *et al.*⁷ Briefly, the network structure emerges as the result of two fusion and two fission reactions between the tips of a set of L dimers. In the model, a dimer tip can connect (disconnect) to other dimer tips forming a network node, but at most three tips can be merged. In this way, the degree k of the

nodes can take only the values $k = 1$ (isolated tip), $k = 2$ (two merged tips) and $k = 3$ (three merged tips); only two fusion processes are allowed: tip-to-tip (two nodes of degree $k = 1$ merge into a node of degree $k = 2$) and tip-to-side (a node of degree $k = 1$ and a node of degree $k = 2$ merge into a node of degree $k = 3$). To each fusion process there is an associated inverse (fission) one. The bias to each process can be written as rates of either fusion or fission²⁰ represented as reaction processes on nodes X_k :



where a_1 (b_1) is the reaction rate for tip-to-tip fusion (fission) process and a_2 (b_2) is the reaction rate for tip-to-side fusion (fission) process. The model can then be implemented as an agent based stochastic dynamics between a set of L reactant objects (dimers), submitted to the above described fusion and fission processes. The dynamics is simulated using Gillespie²¹ algorithm. Nodes participating in a particular event are chosen with equal probability within a list of the nodes with the same degree. Following Ref.⁷ we assumed $b_2 = (3/2)b_1$ and varied the relative rates $c_i = a_i/b_i$.

Sukhorukov *et al.* described in detail the steady state of the dynamics as a function of changes in c_1 and c_2 .⁷ The system admits a plethora of network configurations in parameter space, including fragmented or hyperfused networks resulting from extreme values of fusion and fission activities as well as networks resembling those seen in healthy cells at intermediate values. In passing, notice that more recently this model was reformulated²² to include information on the microtubule cytoskeleton.

In the present work we performed simulations for $L = 15000$, roughly the estimated value for the average number of edges in the control cell images. In every simulation we run the algorithm $3L$ times after which we measured different quantities. This ensured that the distribution of nodes with degree k became stationary. For every set of values of (c_1, c_2) the procedure was repeated 100 times for different sequences of random numbers and the different quantities were averaged over this sample. The different quantities measured were: the average degree $\langle k \rangle$, the average fraction of nodes in the largest cluster $\langle N_g/N \rangle$ and the average cluster size excluding the largest cluster $\langle s \rangle$ (see supplementary material), where the averages were taken both over all the nodes in the network and over different runs.

Data availability. Data from mitochondrial networks is available upon request.

References

1. Gray, M.W., Burger, G., Lang, B.F. Mitochondrial evolution. *Science* **283** 1476-1481 (1999).
2. Friedman, J.R., Nunnari, J. Mitochondrial form and function. *Nature*. **505** 335-343 (2014).
3. Kurz, F.T., Derungs, T., Aon, M.A., O'Rourke, B., Armondas, A.A. Mitochondrial networks in cardiac myocytes reveal dynamic coupling behavior. *Biophysical Journal* **108** 1922-1933 (2015).
4. Aon, M.A., Cortassa, S., O'Rourke B. Percolation and criticality in a mitochondrial network. *Proc Natl Acad Sci USA* **101** 4447-4452 (2004).
5. Collins, T.J., Berridge, M.J., Lipp, P., Bootman, M.D. Mitochondria are morphologically and functionally heterogeneous within cells. *EMBO J* **21** 1616-1627 (2002).
6. Chen, H. & Chan, D.C. Mitochondrial dynamics in mammals. *Curr Top Dev Biol* **59** 119-144 (2004).
7. Sukhorukov, V.M., Dikov, D., Reichert, A.S., Meyer-Hermann, M. Emergence of the mitochondrial reticulum from fission and fusion dynamics. *PLoS Comput Biol* **8** e1002745 (2012).
8. Loson, O.C., Song, Z., Chen, H., Chan, D.C. Fis1, Mff, MiD49, and MiD51 mediate Drp1 recruitment in mitochondrial fission. *Mol Biol Cell* **24** 659-667 (2013).
9. Detmer, S.A. & Chan, D.C. Complementation between mouse Mfn1 and Mfn2 protects mitochondrial fusion defects caused by CMT2A disease mutations. *J Cell Biol* **176** 405-414 (2007).
10. Li, S., Xu, S., Roelofs, B.A., Boyman, L., Lederer, W.J., Sesaki, H., Karbowski, M. Transient assembly of F-actin on the outer mitochondrial membrane contributes to mitochondrial fission. *J Cell Biol* **208** 109-123 (2015).
11. Cocheme, H.M. & Murphy, M.P. Complex I is the major site of mitochondrial superoxide production by Paraquat. *The Journal of Biological Chemistry* **283** 1786-1798 (2008).
12. Castello, P.R., Drechsel, D.A., Patel, M. Mitochondria are a major source of paraquat-induced reactive oxygen species production in the brain. *J Biol Chem* **282** 14186-14193 (2007).

13. Legros, F., Lombes, A., Frachon, P., and Rojo, M. Mitochondrial fusion in human cells is efficient, requires the inner membrane potential, and is mediated by mitofusins. *Mol Biol Cell* **13** 4343-4354 (2002).
14. Rojo, M., Legros, F., Chateau, D., and Lombes, A. Membrane topology and mitochondrial targeting of mitofusins, ubiquitous mammalian homologs of the transmembrane GTPase Fzo. *J Cell Sci* **115** 1663-1674 (2002).
15. Santel, A., & Fuller, M.T. Control of mitochondrial morphology by a human mitofusin. *J Cell Sci* **114** 867-874 (2001).
16. Santel, A., Frank, S., Gaume, B., Herrler, M., Youle, R.J., Fuller, M.T. Mitofusin-1 protein is a generally expressed mediator of mitochondrial fusion in mammalian cells. *J Cell Sci* **116** 2763-2774 (2003).
17. Helguera, P., Seiglie, J., Rodriguez, J., Hanna, M., Helguera, G., Busciglio, J. Adaptive downregulation of mitochondrial function in down syndrome. *Cell Metab* **17** 132-140 (2013).
18. Xu, J. Preparation, culture, and immortalization of mouse embryonic fibroblasts. *Curr Protoc Mol Biol* **70** 1-8 (2005).
19. Baloh, R.H., Schmidt, R.E., Pestronk, A., Milbrandt, J. Altered axonal mitochondrial transport in the pathogenesis of Charcot-Marie-Tooth disease from mitofusin 2 mutations. *J Neurosci* **27** 422-30 (2007).
20. Liu, X., Weaver, D., Shiriha, O., Hajnoczky, G. Mitochondrial “kiss-and-run”: interplay between mitochondrial motility and fusion–fission dynamics. *EMBO J* **28** 3074-3089 (2009).
21. Gillespie, D.T. Exact Stochastic Simulation of Coupled Chemical Reactions. *J. Phys. Chem.* **81** 2340–2361 (1977).
22. Sukhorukov, V.M., Meyer-Hermann, M. Structural heterogeneity of mitochondria induced by the microtubule cytoskeleton. *Scientific Reports* **5** 13924 (2015).

Acknowledgements

This work was partially supported by CONICET (Argentina) through Grants PIP 112-201101-00213, PIP 2015-01-00954 and PICT 2013-3142, and by SECyT (Universidad Nacional de Córdoba, Argentina). DRC thanks the support of Universidad Nacional de San Martín, Argentina.

Author contributions statement

NZ, EZ, PH and DC conceived the experiments; NZ and EZ conducted the experiments; NZ, EZ, SC, OB and DC analyzed the data. All authors reviewed the manuscript.

Additional information

Supplementary information accompanies this paper at <http://www.nature.com/srep>

Competing financial interests: The authors declare no competing financial interests.

How to cite this article: